Published in final edited form as:

J Nucl Med. 2015 November ; 56(11): 1780–1785. doi:10.2967/jnumed.115.160960.

^{18}F-labeled Single-Stranded DNA Aptamer for PET Imaging of Protein Tyrosine Kinase-7 Expression

Orit Jacobson[#1], **Ido D. Weiss**[#2], **Lu Wang**[3], **Zhe Wang**[1], **Xiangyu Yang**[1], **Andrew Dewhurst**[1], **Ying Ma**[1], **Guizhi Zhu**[1], **Gang Niu**[1], **Dale O. Kiesewetter**[1], **Neil Vasdev**[3], **Steven H. Liang**[3,*], and **Xiaoyuan Chen**[1,*]

[1]Laboratory of Molecular Imaging and Nanomedicine, National Institute of Biomedical Imaging and Bioengineering

[2]Laboratory of Molecular Immunology, National Institute of Allergy and Infectious Diseases; National Institutes of Health, Bethesda, MD, USA.

[3]Division of Nuclear Medicine and Molecular Imaging, Massachusetts General Hospital & Department of Radiology, Harvard Medical School, Boston, MA, USA

[#] These authors contributed equally to this work.

Abstract

Protein tyrosine kinase-7 (PTK7), a member of receptor tyrosine kinase superfamily initially identified as colon carcinoma kinase-4 (CCK-4), is highly expressed in various human malignancies. Its expression was found to correlate with aggressive biological behaviors such as increased cell proliferation, invasiveness and migration. Despite the importance and unmet need of imaging PTK7 in vivo, there is currently no clinically-relevant method to visualize tumoral PTK7 expression noninvasively such as PET or SPECT. This study aims to develop a specific, selective and high affinity PET radioligand based on single-stranded DNA (ssDNA) aptamer to address this challenge.

Methods—Sgc8, a 41-oligonucleotide that targets to PTK7, was labeled with F-18 using a two-step radiochemical synthesis, which featured a direct one-step radiofluorination on the distinctive spirocyclic hypervalent iodine(III) precursor to give ^{18}F-fluorobenzyl azide followed by copper mediated “click” conjugation with Sgc8-alkyne. ^{18}F-Sgc8 was evaluated in vitro and in vivo in two cell lines, HCT116 and U87MG, which express high and low amounts of PTK7, respectively.

Results—Sgc8 was labeled efficiently with F-18 in an isolated radiochemical yield of 62 ± 2%, non-decay-corrected (ndc) based on ^{18}F-fluorobenzyl azide. ^{18}F-Tr-Sgc8 was found to possess high affinity binding to both cell lines, with IC_{50} values for HCT116 as 2.7 ± 0.6 nM and U87MG as 16.9 ± 2.1 nM. In vivo PET imaging clearly visualized PTK7 expression in HCT116 xenografted mice with tumor uptake of 0.76 ± 0.09 %ID/g at 30 min post-injection (p.i.) for the subcutaneous tumor model and greater than 1.5 %ID/g for the liver metastasis model. U87MG xenograft tumors had much lower tracer accumulation (0.13 ± 0.06 %ID/g at 30 min p.i.), which was consistent with the lower expression of PTK7 in this tumor model. The labeled aptamer was

[*] Correspondence: Liang.Steven@mgh.harvard.edu; shawn.chen@nih.gov.

rapidly cleared from the blood through the kidneys and bladder to give high tumor-to-blood and tumor-to-muscle ratios of 7.29 ± 1.51 and 10.25 ± 2.08, respectively.

Conclusions—The F-18 radiolabeling methodology shown here is a very robust procedure for labeling aptamers and similar chemical moieties, and can be applied to many different targets. Quantification of PTK7 using ^{18}F-Tr-Sgc8 may be suitable for clinical translation and might help in the future to select and monitor appropriate therapies.

Keywords

PTK7; PET Imaging; F-18; Click chemistry; ssDNA aptamer

Protein tyrosine kinase-7 (PTK7), a member of receptor tyrosine kinase superfamily initially identified as colon carcinoma kinase-4 (CCK-4), is highly expressed in various human malignancies (1, 2). Encoding fragments of PTK7 were initially identified in mRNA from human melanocytes, and, subsequently PTK7 was fully cloned from a colon cancer tissue (3, 4). The protein consists of seven immunoglobulin-like extracellular domains, a single transmembrane domain, and cytoplasmic domain with tyrosine kinase homology that lacks vital catalytic activity but maintains signal transduction (4–7).

Deletion of the PTK7 gene in mice is lethal, and the embryos developed many defects in the gastrulating cell process. Subsequently, it was found that the protein PTK7 is conserved through evolution and plays a pivotal role in cell movement and localization during embryonic development (5, 7–9). Endogenous ligands of PTK7 have not yet been identified.

As indicated above, PTK7 was cloned from colon cancer, although not expressed in normal colon. Further research showed that it is also expressed by other cancers including gastric, acute myeloid leukemia (AML), lung and glioblastoma overexpressing CD44 (6, 10–14). The role of PTK7 in cancer is controversial, perhaps because it might play different roles in the biology of cancers that arise from different tissues. Interestingly, while in some cancers PTK7 is upregulated and believed to promote tube formation, migration, angiogenesis and invasiveness of endothelial cells (8), PTK7 is found to be downregulated in other cancers and/or during advanced stages of the cancer (15–18). Moreover, in lung squamous cell carcinoma it was suggested to be a tumor suppressor, and when it was transfected into lung cancer cell lines it reduced cell proliferation, invasion, and migration (18). Hence, PTK7 may be a pharmaceutical target in some cancers; however, its role in each specific targeted cancer requires exploration.

One of the limitations in studying PTK7 is the absence of a method for evaluating and quantifying the expression of PTK7 protein in cancer tissue non-invasively over time. Currently there is no radioactive tracer that will allow such studies. To address this need, we developed a positron emission tomography (PET) tracer that targets PTK7, based on a known aptamer sequence named Sgc8 (19, 20).

Aptamers are short single-stranded DNA or RNA oligonucleotides that possess high selectivity and specificity to a target molecule. The specific binding of aptamers to their targets depends on a distinctive and unique three dimensional folding, and they display high

affinities that are similar to antibodies. In contrast to antibodies, the relatively small molecular weight of aptamers allows rapid penetration into tissues and fast clearance from the blood to give higher target-to-background ratio at early time points. Therefore, aptamers are attractive candidates for in vivo PET imaging (21, 22).

Sgc8 aptamer contains 41 oligonucleotides and was selected by cell based systematic evolution of ligands by exponential enrichment (SELEX) against human T lymphoblast CCRF-CEM cells (19, 20). The target of the Sgc8 aptamer was deduced as PTK7 using biotin-Sgc8 and magnetic streptavidin beads for isolation of biomarker complexes and LC-MS/MS to identify the complexed protein. Here we describe radiolabeling of Sgc8 with the PET isotope F-18 *via* a click chemistry reaction and evaluation of ^{18}F-Tr-Sgc8 ex vivo and in vivo for stability and ability to image and quantify PTK7 expression in different mouse tumor models.

MATERIALS AND METHODS

General

Supplemental materials describe the procedures for radiolabeling of ^{18}F-fluorobenzyl azide, assays of PTK7 expression, cell binding procedures, and magnetic resonance imaging (MRI).

Radiochemistry

Sgc8-alkyne aptamer (150 μg in 15 μL of water) were mixed in an Eppendorf tube with 0.7 mg of $CuSO_4 \cdot 5H_2O$ in 20 μL of water and 5.6 mg of sodium ascorbate in 200 μL 0.1M borate buffer (pH 8.6). Then, 50 μL of ^{18}F-benzylazide (5-6 mCi, 185-222 MBq) in CH_3CN were added, followed by a short vortex and incubation at 37 °C for 15 min. The crude reaction mixture was loaded onto a NAP5 column and eluted with 0.5 mL fractions of H_2O. The radiochemical yield (RCY) of ^{18}F-Tr-Sgc8 was calculated from the combined radioactivity of fractions 4 and 5 divided by the initial quantity of ^{18}F-fluorobenzyl azide without decay correction. Radiosynthesis of ^{18}F-fluorobenzyl azide and quality control of ^{18}F-Tr-Sgc8 was described in the supplemental materials.

Biology

Tumor Xenograft Models—Mice were inoculated subcutaneously with 5×10^6 cells of either HCT116 or U87MG on the right shoulder (n = 5 per group). The tumors were allowed to develop for 2.5-3 weeks prior to PET imaging and biodistribution studies.

Tumor Metastasis Model—The mice were anesthetized with isoflurane/O_2 (1.5–2% v/v) inhalation. For surgical hepatic injection, a small (0.5 to 1 cm) incision was made in the skin above the liver. The peritoneal membrane was gently lifted and a small incision was made, avoiding any injury to the liver. Then 2 μL of 1×10^5 HCT116 cells pre-mixed with Matrigel (BD Biosciences) at 1:1 ratio were injected to the liver of each mouse (n = 4) using a 10 μL syringe (Hamilton) fitted with a 31-gauge needle. Following injection of the cells, the syringe was held for 1 - 2 min, and then withdrawn from the tissue. The abdominal wall

was sutured using a 6.0 vicryl absorbable suture (Ethicon). The tumors were allowed to develop for 4 - 5 weeks prior to PET studies.

PET and Biodistribution Studies—Tumor-bearing mice were injected intraperitoneally with 0.5 mL saline 10 min before intravenous injection of 100 μCi (3.7 MBq) of ^{18}F-Tr-Sgc8 (8 μg, 0.6 nmol) in order to facilitate urine clearance. For blocking studies, 100 μCi (3.7 MBq) of ^{18}F-Tr-Sgc8 was co-injected with 100-fold excess (800-850 μg, 60-65 nmol) of unlabeled Sgc8-alkyne (n = 3). 5-10 min PET scans were performed using an Inveon scanner (Siemens Medical Solutions) at 30 min and 1 h post injection (p.i.). ASI Pro VM™ software was used for image analysis. Regions of interest were drawn for each organ on the coronal images to calculate %ID/g, assuming a density of 1 g/cm^3 for all tissues. After the 1 h PET scan, the mice were sacrificed; organs were harvested and wet-weighed. The radioactivity of samples was measured using a gamma-counter (Wallac Wizard 1480, PerkinElmer), and the results were expressed as percentages of the injected dose per gram of tissue (%ID/g).

^{18}-F-Tr-Sgc8 Stability in Blood and Urine—To study the stability in blood, 3.7-5.5 MBq (100-150 μCi) of ^{18}F-Tr-Sgc8 were injected into each mouse. At 5 min after injection, the mice were sacrificed and blood was collected in EDTA containing tubes. The plasma was separated from red blood cells by centrifuging at 3,500 rpm for 5 min. The plasma was incubated for 5 min at 95°C, followed by centrifugation at 14,000 rpm for 5 min.

An aliquot of 20-30 μL of each sample was injected into HPLC and 1 min fractions were collected for 30 min using a fraction collector. The radioactivity of each fraction was measured using a gamma-counter. Urine was collected at 30 min and 1 h time points. An aliquot of 20-30 μL was injected into HPLC. Procedures describing in vitro stability studies of ^{18}F-Tr-Sgc8 are included in the supplemental materials.

Statistical Analysis

Results were presented as mean ± standard deviation (SD). Group comparisons were made using Student's *t* test for unpaired data. *P* values <0.05 were considered statistically significant.

RESULTS

Chemistry and Radiochemistry

Sgc8 aptamer, consisting of 41 oligonucleotides, was modified at the 5' with a terminal hexynyl group (Figure 1). Conjugation of unlabeled Sgc8-alkyne to 1.5 equivalent of fluorobenzyl azide in the presence of excess amount of $CuSO_4 \cdot 5H_2O$ and sodium ascorbate resulted in full conversion into the desired product (Supplemental Figure 1) which was verified by LC-MS analysis (Supplemental Figure S2). The automated radiochemical synthesis of ^{18}F-fluorobenzyl azide was achieved using an aromatic fluoride substitution on a novel spirocyclic hypervalent iodine(III) precursor (24) (**1**, Figure 1). The labeling yield was 32 ± 3% (n = 5), non-decay-corrected (ndc) based on F-18 activity. ^{18}F-fluorobenzyl azide was obtained with high specific activity (SA) of 3.5-4 Ci/μmol (129.5-148 Gbq/μmol,

n = 5). Because of its volatility, ^{18}F-fluorobenzyl azide cannot be concentrated *via* solvent evaporation and, therefore, was used directly from the CH_3CN elution of the final C-18 Sep-Pak. For aptamer conjugation, 50 μL of ^{18}F-fluorobenzyl azide were used, and attempts to increase the volume (and activity) resulted in lower labeling efficiency (Supplemental Material Table S1).

Reaction of Sgc8-alkyne with ^{18}F-fluorobenzyl azide was conducted as described for the unlabeled fluorobenzyl azide, and similarly, resulted in formation of one major and desired product. The high SA ^{18}F-fluorobenzyl azide was all consumed (Supplemental Figure S3). Typically, 150 μg (11 nmol) of Sgc8-alkyne were used for radiolabeling. Attempts to minimize the amount of the aptamer to 50 μg (3.8 nmol) per reaction resulted in the same conversion (Supplemental Material Table S1). However, using 13 μg (1 nmol) of aptamer, resulted in only 48% conversion into the desired labeled aptamer (Table S1). The crude reaction was purified on NAP5 column to give ^{18}F-Tr-Sgc8 with radiochemical purity >95% and RCY of 62 ± 2% ndc (n=5) based on initial ^{18}F-fluorobenzyl azide radioactivity. The final specific activity of the labeled aptamer, calculated by dividing the obtained radioactivity by the total mass of Sgc8-alkyne used for the reaction, was 182-198 mCi/μmol (6.7-7.3 GBq/μmol).

Biology

PTK7 Expression by HCT116 and U87MG Cells—Flow cytometry and Western blot analysis showed higher expression by HCT116 than by U87MG cells (Figures 2A and 2B). ^{18}F-Tr-Sgc8 binding affinity to HCT116 was slightly better (2.7 ± 0.6 nM, n = 2) than U87MG (16.9 ± 2.1 nM, n = 2, Figure 2C). The amount of ^{18}F-Tr-Sgc8 captured on each cell line also correlated with expression levels of PTK7 (Figure 2C). Western blot analysis of proteins from tumor lysates showed that HCT116 retained PKT7 expression in vivo, while the protein level was almost undetected in U87MG tumor lysate (Figure 2D).

PTK7 Imaging in Tumor-Bearing Mice—^{18}F-Tr-Sgc8 uptakes at all the time points examined were significantly higher in HCT116 than those in U87MG xenografts (0.76 ± 0.09 *vs.* 0.13 ± 0.06 %ID/g at 30 min p.i. and 0.54 ± 0.12 *vs.* 0.19 ± 0.06 %ID/g at 1 h p.i., Figures 3A and B). ^{18}F-Tr-Sgc8 uptake in the HCT116 tumors slightly decreased between 30 min and 1 h p.i. The receptor specificity of ^{18}F-Tr-Sgc8 to PTK7 was tested by blocking studies in the HCT116 tumor model. By co-injection of ^{18}F-Tr-Sgc8 with excess amount of Sgc8-alkyne, the uptake was decreased by approximately 80% (Figures 3A). Moreover, ^{18}F-Tr-Sgc8 had faster clearance through the urine when injected with an excess of cold mass. Although ^{18}F-Tr-Sgc8 had undesired nonspecific uptake in metabolic organs, including gallbladder, intestine, and kidneys (Figure 3C), ^{18}F-Tr-Sgc8 showed fast clearance from the blood and the optimal imaging time was 1 h p.i. with higher tumor contrast and tumor-to-blood and tumor-to-muscle ratios of 7.29±1.51 and 10.25±2.08, respectively. ^{18}F-Tr-Sgc8 had some uptake in the bone (0.37±0.06 %ID/g at 1 h pi) which was not reduced in the co-injection experiments, suggesting the possibility of slight de-fluorination in vivo.

The ability of ^{18}F-Tr-Sgc8 to image tumors in the liver, kidneys and peritoneal sites was also evaluated (Figure 4) using a metastatic tumor model. Inoculation of HCT116 cells into the

liver resulted in tumors not only in the liver, but also in the kidneys and peritoneum, as confirmed by MRI and necropsy. Peritoneal tumors might have formed from some spill of cells from the injection site. The uptake of ^{18}F-Tr-Sgc8 in metastatic lesions in the peritoneum and the kidneys (approximately 1.5-2 %ID/g at 1 h pi, Figure 4 and Supplemental Figure S4) was higher than that of subcutaneous tumors. Liver lesions had the uptake of 0.5-0.7 %ID/g and were very small (16-20 mg). This might be due to differential blood flow and vascularity in subcutaneous tumors *vs.* abdominal/liver tumors.

Ex Vivo and In Vivo Stability of ^{18}F-Tr-Sgc8—^{18}F-Tr-Sgc8 stability was initially evaluated ex vivo in mouse serum. An aliquot of the serum was taken at 30 min and 1 h post-incubation and the radioactivity was diluted using saline. The aptamer readily bound to serum components and, thus, most of the radioactivity remained in the pellet. Denaturation of the proteins at 95 °C increased aptamer recovery, but remained low with 80% of ^{18}F-Tr-Sgc8 in the pellet. To evaluate the formation of small molecules from aptamer degradation, the mixture of ^{18}F-Tr-Sgc8 in serum was loaded onto a NAP5 column and the activity of different fractions was measured. Most of the activity (>80%) came off the column in fraction 4, suggesting that the aptamer was intact but did not exclude its binding to proteins. Gel electrophoretic analysis showed that no significant amount of metabolites was formed in the serum up to 1 h incubation (Figure 5A). Activity extracted from 30 min time-point was injected into HPLC (Supplemental Figure S5A); no degradation of the labeled aptamer was observed. ^{18}F-Tr-Sgc8 stability was further evaluated in vivo in the blood and urine. Since ^{18}F-Tr-Sgc8 rapidly clears from the blood, the blood was withdrawn at 5 min p.i. An aliquot of the extracted plasma was injected into HPLC and the major component in this aliquot eluted at 19.7 min, two minutes later than the retention time of ^{18}F-Tr-Sgc8 (Figure 5B, Supplemental Figure S5B). Moreover, urine samples that were taken 30 min and 1 h p.i. showed no traces of ^{18}F-Tr-Sgc8 but the appearance of two new peaks; one is more hydrophilic with retention time of 15.2 min and the other is more hydrophobic, with a retention time of 24.9 min (Supplemental Figure S5C). It is important to emphasize that traces of unlabeled aptamer could be detected in the urine samples, according to the UV chromatogram (Supplemental Figure S5C).

Discussion

PTK7 expression was shown to have controversial roles in different tumors, and it seems to be dependent on several conditions, which are in part tissue specific. Hence, the study of clinical significance and function of PTK7 in cancers is an on-going research effort. However, it is at least partially hampered by the lack of a reliable method to evaluate PTK7 expression non-invasively in whole tumors (12, 26). An example of the above mentioned controversy is a study done in adenocarcinoma patients that suggests that PTK7 expression predicts a favorable prognosis (13). On the other hand, evaluation of AML patients showed that PTK7-positive patients had higher resistance to anthracycline-based cancer chemotherapy and had a significantly reduced rate of relapse-free survival (27). The methods for determination of PTK7 expression by tumors and tumor cells are limited to immunohistochemistry and PCR, which are conducted on biopsy samples. A method to evaluate the receptor expression in the whole tumor non-invasively could be a great asset to

study the significance and functions for PTK7 in a wide variety of cancers. In this study we address this unmet need through the development of a PET tracer for PTK7 based on a DNA aptamer.

We have previously published the labeling of Tenascin-C aptamer with F-18 *via* N-succinimidyl 4-^{18}F-fluorobenzoate (^{18}F-SFB) (25), which resulted in very low RCY. In an effort to improve radiochemical yields for this study, we applied the click reaction between ^{18}F-fluorobenzylazide and Sgc8-alkyne. The radiosynthesis of ^{18}F-fluorobenzylazide prepared *via* spirocyclic iodonium ylide and the subsequent click reaction with Sgc8 proved to be very robust and reliable and resulted in high RCY. While usage of 11 nmol of Sgc8-alkyne for the click reaction provided complete conversion of ^{18}F-fluorobenyzlazide, small amount of Sgc8-alkyne (as little as 1 nmol) also resulted in nearly 50% conversion into the labeled aptamer (Supplemental Table S1), which is obviously better than ^{18}F-SFB conjugation yields realized for Tenascin C aptamer. Our preliminary in vivo PET studies showed suboptimal images when a small mass of aptamer was injected into the mice, whereas, higher mass amounts resulted in better images **(**Supplemental Figure S6**)**. This may be due to the very rapid clearance of the radioactive aptamer through gallbladder and kidneys. We believe that an increase in injected mass slowed the clearance and/or metabolism just enough to allow higher uptake in target tissues. Indeed our optimized conditions used 11 nmol of Sgc8-alkyne and purification of radiolabeled product from unreacted precursor was not necessary. This phenomenon of lower uptake in gallbladder coupled with higher uptake in the target organ/tumor as a function of injected mass is fascinating and might be beneficial to other tracers. However, our experience is limited to this aptamer, and further studies on this phenomenon should be carried out with other tracers. If this phenomenon is seen with other tracers, it suggests that tracer development studies should also include experiments to optimize the ratio of unlabeled-to-labeled tracer ratio, which will give best image in regard to gallbladder uptake and target uptake. In our standard radiolabeling method, ^{18}F-Tr-Sgc8 was injected with 5-8 μg of unreacted Sgc8-alkyne per mouse.

PET studies showed specific accumulation of ^{18}F-Tr-Sgc8 in HCT116 tumor-bearing mice (Figures 3A and 3C) that express high level of PTK7 (Figure 2D). U87MG tumors express lower level of PTK7 (Figure 2D) and had relatively lower uptake of ^{18}F-Tr-Sgc8 (Figure 3B). The specificity of the uptake was demonstrated by an 80% inhibition of uptake upon co-injection of 60 nmol of Sgc8-alkyne. Moreover, images of ^{18}F-Tr-Sgc8 uptake were obtained following inoculation of HCT116 cells into the liver (Figure 4). Although there was relatively high background due to uptake in the gallbladder, intestine and kidneys, the tumors in the liver, peritoneum and above the kidneys were clearly visualized with good tumor-to-background ratios (Figure 4 and Supplemental Figure S4 and Supplemental Movie S1). The uptake in the intestine, which was higher than the uptake in the tumor, suggests that ^{18}F-Tr-Sgc8 is not suitable for imaging PTK7 expression by colon tumors. Lower uptake seen in the subcutaneous tumors of HCT116 when compared to the tumor lesions elsewhere might be due to different blood flow and not attributed to different receptor expression (Figure 2D).

In order to gain some insight into the biological clearance mechanism, we compared the biodistribution of ^{18}F-Tr-Sgc8 with ^{18}F-SFB labeled Sgc8. Radiolabeling of Sgc8 with ^{18}F-SFB required acquisition of Sgc8 with a primary amine at the 5'-end. Formation of the benzyl triazole ring during the click reaction makes ^{18}F-Tr-Sgc8 more hydrophobic than aptamer conjugated to ^{18}F-SFB. ^{18}F-Tr-Sgc8 had considerable uptake in the intestine (Figure 3C) and also showed some bone uptake (0.37 ± 0.06 %ID/g), which suggests metabolic de-fluorination (Figure 3C) or, perhaps, formation of F-18 clicked phosphate metabolite which accumulates in the bone. When Sgc8 was labeled with ^{18}F-SFB, the bone uptake was much lower (0.11±0.02 %ID/g at 1 h p.i. (Supplemental Figure S7**).** A more detailed study of the effect of different chemical linkers on de-fluorination may be required.

^{18}F-Tr-Sgc8 stability was further tested in vitro in mouse serum and in vivo in blood and urine. ^{18}F-Tr-Sgc8 proved to be stable in mouse serum with no significant metabolite formation (Figure 5A). About 25-30% of the total injected radioactivity was collected from the urine at 30 min p.i., which indicated a fast clearance of ^{18}F-Tr-Sgc8 through kidneys. Radio-HPLC showed two small molecule based components but no parent ^{18}F-Tr-Sgc8. These products were probably caused by the metabolism of the phosphodiester bond between the aptamer and/or the prosthetic group (Supplemental Figure S5C). Typically large molecules such as aptamers or proteins are eluted in fraction 4 (0.75 – 1.0 mL); however, we observed most of the radioactivity remained on the column and could only elute with extensive washing. This is indicative of small molecules. One would be an alcohol that is consistent with the more hydrophobic peak seen in HPLC at 24.9 min (Supplemental Figure S5C); and the other would contain a phosphate group and peaked at 15.4 min (Supplemental Figure S5C). Upon analysis by LC-MS, we observed not only unreacted Sgc8 but also one large molecule with a deconvoluted mass of 18 kDa, which is 6 kDa higher than the unreacted Sgc8 (Supplemental Figure S8). This supports our hypothesis that the aptamer or its fragments bind to some blood component (lipids/small proteins) in vivo.

It is important to note that although we observed some degradation of the ^{18}F-Tr-Sgc8 and/or the unreacted Sgc8, it does not hamper the use of ^{18}F-Tr-Sgc8 as a PET imaging tracer in the visualization and quantification of PTK-7 expression of the tumors in vivo, evidenced by the rapid clearance of ^{18}F-Tr-Sgc8 from the blood *via* the kidneys into urine, and excellent target-to-background signal ratios.

CONCLUSION

^{18}F labeling methodology that uses 4-[^{18}F]fluorobenzyl azide is efficient for labeling aptamers and other biomolecules. ^{18}F-Tr-Sgc8 was specific and sensitive to the PTK7 level as shown by the higher uptake in HCT116 tumors with high expression of PTK7 compared to low uptake in U87MG tumors with low expression of the protein. Quantification of PTK7 using ^{18}F-Sgc8 will be valuable for future studies of PTK7 expression and its different roles in various cancers. It is expected that this tracer will be suitable for clinical translation and help select and monitor appropriate therapies that are PTK7 related.

Supplementary Material

Refer to Web version on PubMed Central for supplementary material.

ACKNOWLEDGMENT

This work was supported by the intramural research program of the National Institute of Biomedical Imaging and Bioengineering (NIBIB), National Institutes of Health (NIH).

REFERENCES

1. Jiang G, Zhang M, Yue B, et al. PTK7: a new biomarker for immunophenotypic characterization of maturing T cells and T cell acute lymphoblastic leukemia. Leuk Res. 2012; 36:1347–1353. [PubMed: 22898210]
2. Jin J, Ryu HS, Lee KB, Jang JJ. High expression of protein tyrosine kinase 7 significantly associates with invasiveness and poor prognosis in intrahepatic cholangiocarcinoma. PLoS One. 2014; 9:e90247. [PubMed: 24587299]
3. Lee ST, Strunk KM, Spritz RA. A survey of protein tyrosine kinase mRNAs expressed in normal human melanocytes. Oncogene. 1993; 8:3403–3410. [PubMed: 8247543]
4. Park SK, Lee HS, Lee ST. Characterization of the human full-length PTK7 cDNA encoding a receptor protein tyrosine kinase-like molecule closely related to chick KLG. J Biochem. 1996; 119:235–239. [PubMed: 8882711]
5. Boudeau J, Miranda-Saavedra D, Barton GJ, Alessi DR. Emerging roles of pseudokinases. Trends Cell Biol. 2006; 16:443–452. [PubMed: 16879967]
6. Mossie K, Jallal B, Alves F, Sures I, Plowman GD, Ullrich A. Colon carcinoma kinase-4 defines a new subclass of the receptor tyrosine kinase family. Oncogene. 1995; 11:2179–2184. [PubMed: 7478540]
7. Lu X, Borchers AG, Jolicoeur C, Rayburn H, Baker JC, Tessier-Lavigne M. PTK7/CCK-4 is a novel regulator of planar cell polarity in vertebrates. Nature. 2004; 430:93–98. [PubMed: 15229603]
8. Shin WS, Maeng YS, Jung JW, Min JK, Kwon YG, Lee ST. Soluble PTK7 inhibits tube formation, migration, and invasion of endothelial cells and angiogenesis. Biochem Biophys Res Commun. 2008; 371:793–798. [PubMed: 18471990]
9. Peradziryi H, Tolwinski NS, Borchers A. The many roles of PTK7: a versatile regulator of cell-cell communication. Arch Biochem Biophys. 2012; 524:71–76. [PubMed: 22230326]
10. Saha S, Bardelli A, Buckhaults P, et al. A phosphatase associated with metastasis of colorectal cancer. Science. 2001; 294:1343–1346. [PubMed: 11598267]
11. Gorringe KL, Boussioutas A, Bowtell DD. Novel regions of chromosomal amplification at 6p21, 5p13, and 12q14 in gastric cancer identified by array comparative genomic hybridization. Genes Chromosomes Cancer. 2005; 42:247–259. [PubMed: 15611932]
12. Lin Y, Zhang LH, Wang XH, et al. PTK7 as a novel marker for favorable gastric cancer patient survival. J Surg Oncol. 2012; 106:880–886. [PubMed: 22585737]
13. Endoh H, Tomida S, Yatabe Y, et al. Prognostic model of pulmonary adenocarcinoma by expression profiling of eight genes as determined by quantitative real-time reverse transcriptase polymerase chain reaction. J Clin Oncol. 2004; 22:811–819. [PubMed: 14990636]
14. Liu Q, Zhang C, Yuan J, et al. PTK7 regulates Id1 expression in CD44-high glioma cells. Neuro Oncol. 2015; 17:505–515. [PubMed: 25204555]
15. Wang H, Li G, Yin Y, et al. PTK7 protein is decreased in epithelial ovarian carcinomas with poor prognosis. Int J Clin Exp Pathol. 2014; 7:7881–7889. [PubMed: 25550828]
16. Easty DJ, Mitchell PJ, Patel K, Florenes VA, Spritz RA, Bennett DC. Loss of expression of receptor tyrosine kinase family genes PTK7 and SEK in metastatic melanoma. Int J Cancer. 1997; 71:1061–1065. [PubMed: 9185712]
17. Behbahani TE, Thierse C, Baumann C, et al. Tyrosine kinase expression profile in clear cell renal cell carcinoma. World J Urol. 2012; 30:559–565. [PubMed: 21969129]

18. Kim JH, Kwon J, Lee HW, et al. Protein tyrosine kinase 7 plays a tumor suppressor role by inhibiting ERK and AKT phosphorylation in lung cancer. Oncol Rep. 2014; 31:2708–2712. [PubMed: 24789704]

19. Shangguan D, Li Y, Tang Z, et al. Aptamers evolved from live cells as effective molecular probes for cancer study. Proc Natl Acad Sci U S A. 2006; 103:11838–11843. [PubMed: 16873550]

20. Shangguan D, Cao Z, Meng L, et al. Cell-specific aptamer probes for membrane protein elucidation in cancer cells. J Proteome Res. 2008; 7:2133–2139. [PubMed: 18363322]

21. Jacobson O, Chen X. Interrogating tumor metabolism and tumor microenvironments using molecular positron emission tomography imaging. Theranostic approaches to improve therapeutics. Pharmacol Rev. 2013; 65:1214–1256. [PubMed: 24064460]

22. Shi H, He X, Wang K, et al. Activatable aptamer probe for contrast-enhanced in vivo cancer imaging based on cell membrane protein-triggered conformation alteration. Proc Natl Acad Sci U S A. 2011; 108:3900–3905. [PubMed: 21368158]

23. Culbert PA, Adam MJ, Hurtado ET, et al. Automated synthesis of [^{18}F]FDG using tetrabuthylammonium bicarbonate. Appl Radiat Isot. 1995; 46:887–891.

24. Rotstein BH, Stephenson NA, Vasdev N, Liang SH. Spirocyclic hypervalent iodine(III)-mediated radiofluorination of non-activated and hindered aromatics. Nat Commun. 2014; 5:4365. [PubMed: 25007318]

25. Jacobson O, Yan X, Niu G, et al. PET imaging of Tenascin-C with a radiolabeled single-stranded DNA aptamer. J Nucl Med. 2015; 56:616–621. [PubMed: 25698784]

26. Muller-Tidow C, Schwable J, Steffen B, et al. High-throughput analysis of genome-wide receptor tyrosine kinase expression in human cancers identifies potential novel drug targets. Clin Cancer Res. 2004; 10:1241–1249. [PubMed: 14977821]

27. Prebet T, Lhoumeau AC, Arnoulet C, et al. The cell polarity PTK7 receptor acts as a modulator of the chemotherapeutic response in acute myeloid leukemia and impairs clinical outcome. Blood. 2010; 116:2315–2323. [PubMed: 20558616]

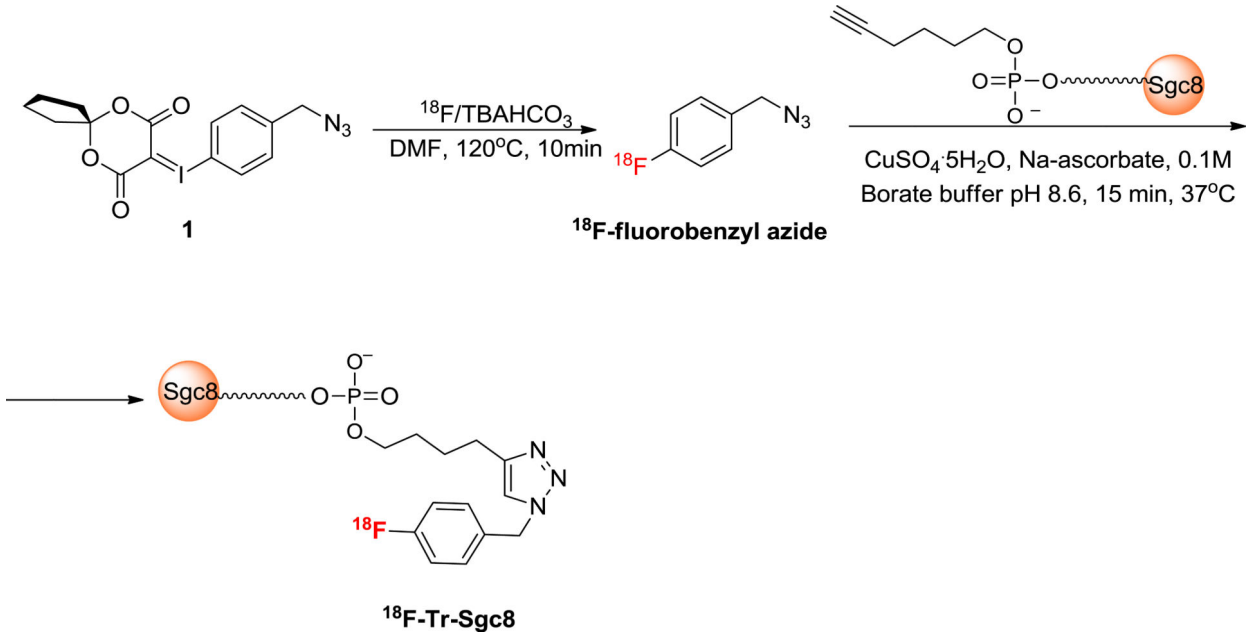

Figure 1.
Radiosynthesis of ^{18}F-Tr-Sgc8.

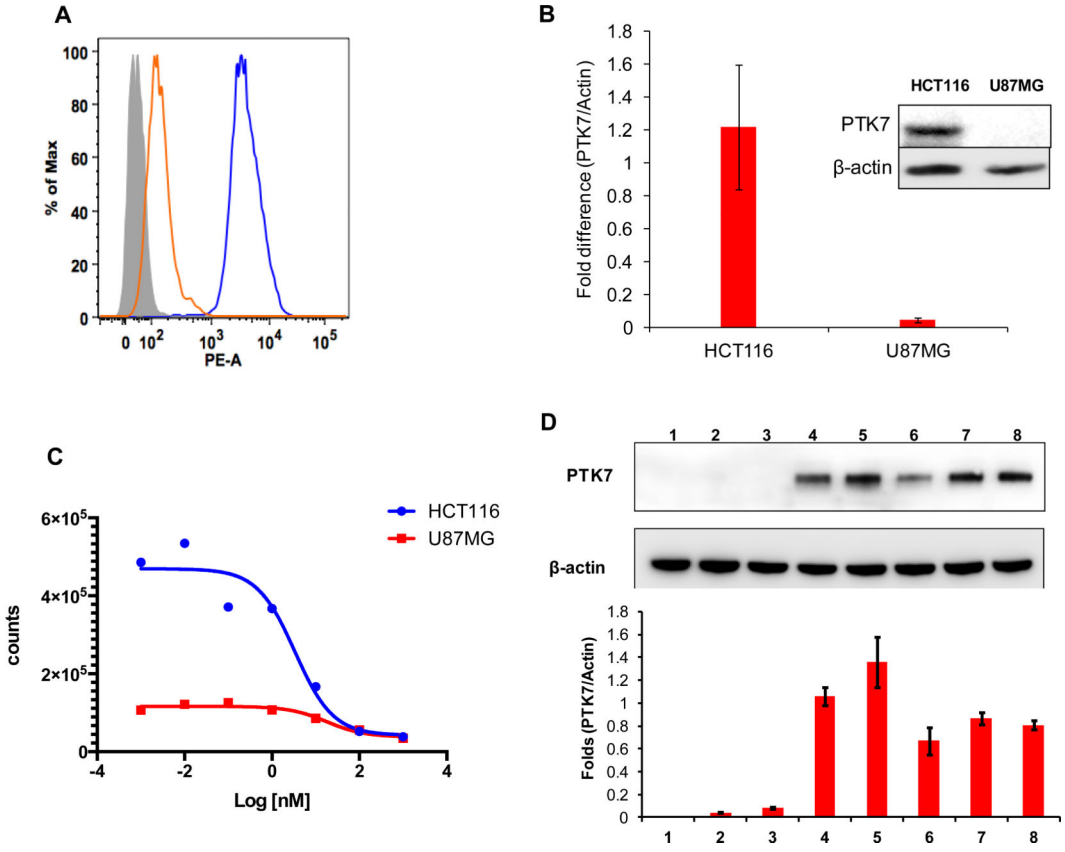

Figure 2.

(A) Flow cytometry of PTK7 expression results for HCT116 and U87MG cell lines. (B) Western blot analysis of PTK7 and β-actin expression by cells (C) Binding affinities of ^{18}F-Tr-Sgc8 in HCT116 and U87MG cells. (D) Representative Western blot analysis of PTK7 and β-actin expression by liver (1), intestine (2), U87MG tumor (3), HCT116 peritoneal metastasis (4), subcutaneous HCT116 tumor (5), HCT116 kidney metastasis (6), HCT116 liver tumor (7) and HCT116 peritoneal wall metastasis (8) (two upper panels) and quantitative results of PTK7/β-actin ratio from three Western blots (lower panel).

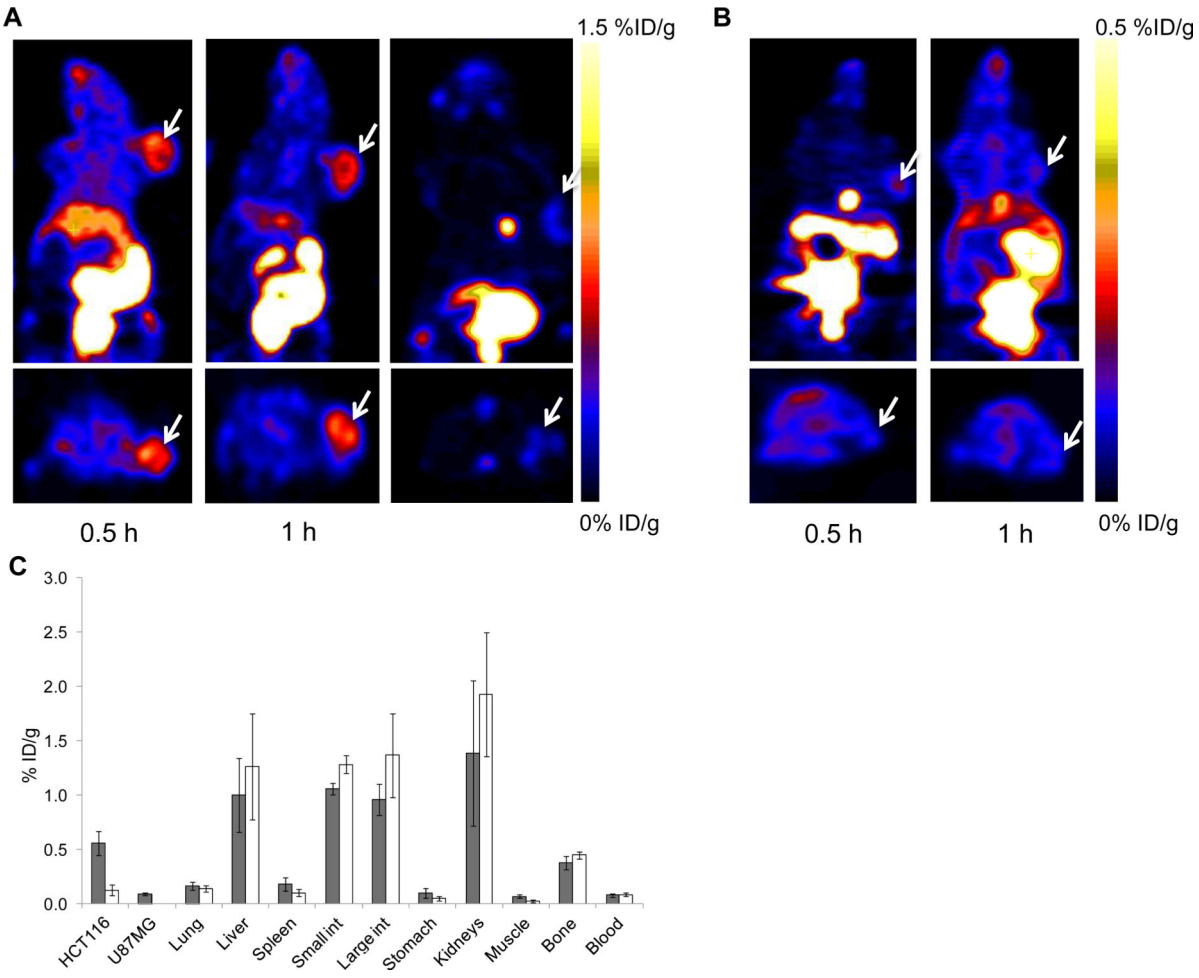

Figure 3.

(A) Representative coronal (upper) and transaxial (lower) PET images of mice bearing HCT116 xenografts injected with ^{18}F-Tr-Sgc8 at 30 min (right panel), 1 h (middle panel) and 1 h co-injection with an excess amount of unlabeled aptamer (left panel). (B) Representative coronal (upper) and transaxial (lower) PET images of mice bearing U87MG tumors at 30 min and 1 h p.i. of ^{18}F-Tr-Sgc8 (100 μCi) and (C) Biodistribution of ^{18}F-Tr-Sgc8 at 1 h post-injection without additional of unlabeled aptamer (grey column) and with addition of unlabeled aptamer (white columns).

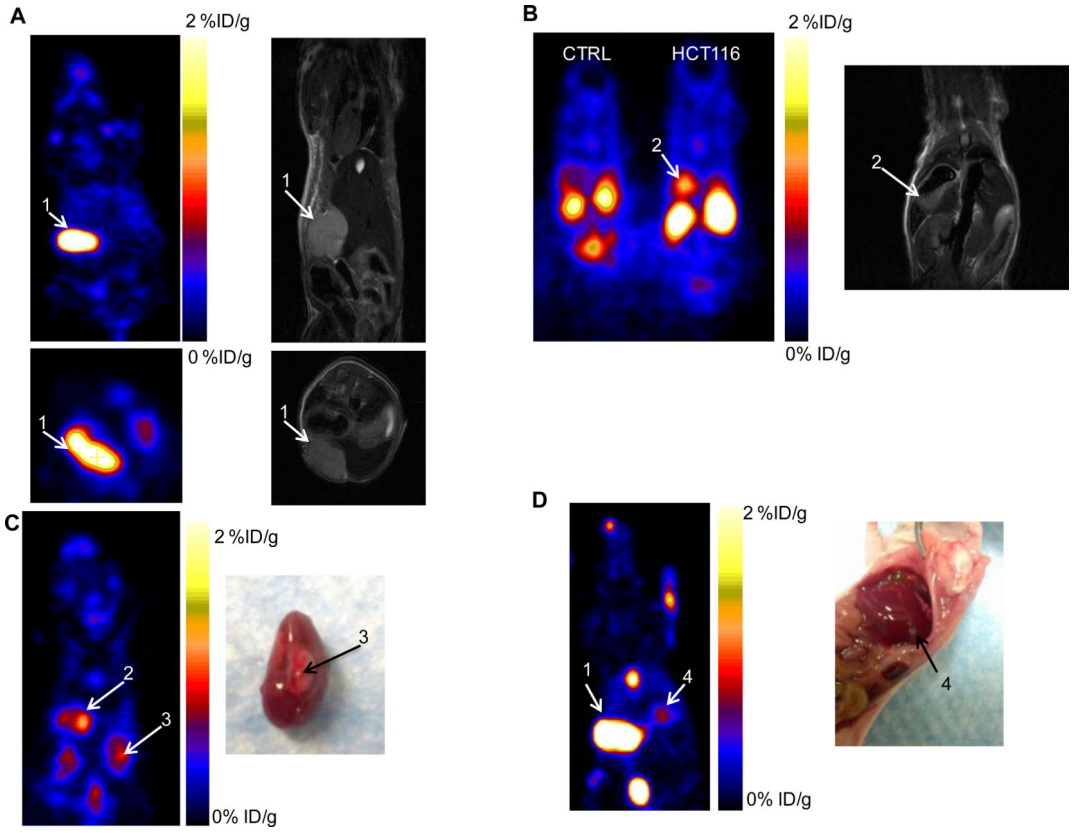

Figure 4.

(A, B) Representative PET and MR images of mice with metastatic HCT116 tumors at 1 h p.i. of ^{18}F-Tr-Sgc8. (C, D) PET image and necropsy of the indicated tumors. Arrows and numbers indicate the different tumors shown in the PET image and matching MRI / necropsy.

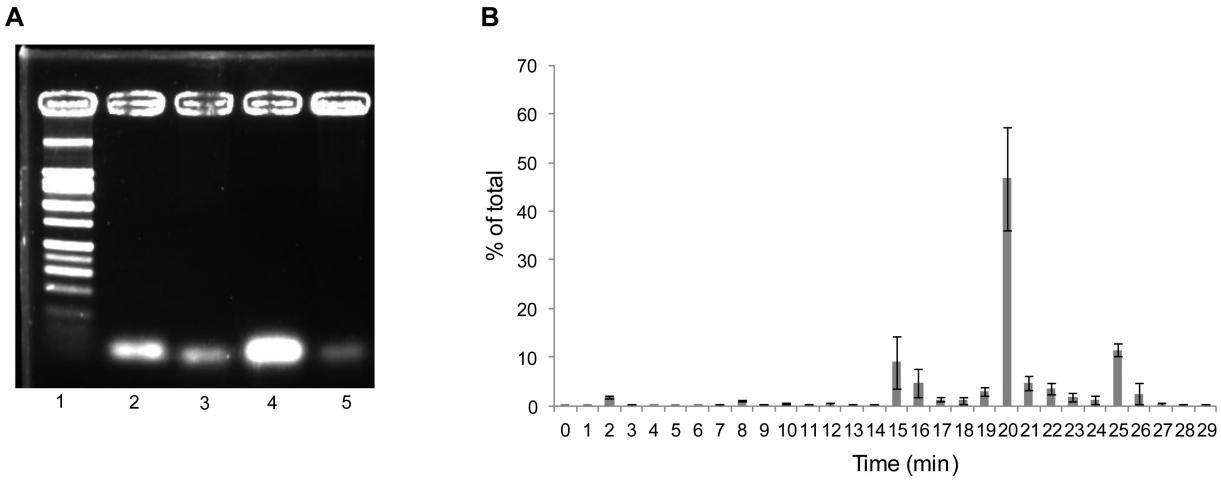

Figure 5.

(A) Representative agarose gel electrophoresis of ^{18}F-Tr-Sgc8 post mouse serum incubation and extraction as described in materials and methods. Lane 1 – ladder; lane 2 – aptamer standard; lane 3 – 30 min incubation; lane 4 – 1 h incubation post NAP5; lane 5 – 1 h incubation. (B) In vivo blood stability analysis of ^{18}F-Tr-Sgc8 by gamma counter.